# Supporting Information

## Synthesis of hierarchical structured $Fe_2O_3$ rod clusters with numerous empty nanovoids via the Kirkendall effect and their electrochemical properties for lithium-ion storage

Seung-Keun Park, Jae Hun Choi and Yun Chan Kang*

Department of Materials Science and Engineering, Korea University, Anam-Dong, Seongbuk-Gu, Seoul 136-713, Republic of Korea.

*Correspondence authors. E-mail: yckang@korea.ac.kr (Yun Chan Kang, Fax: (+82) 2-928-3584)

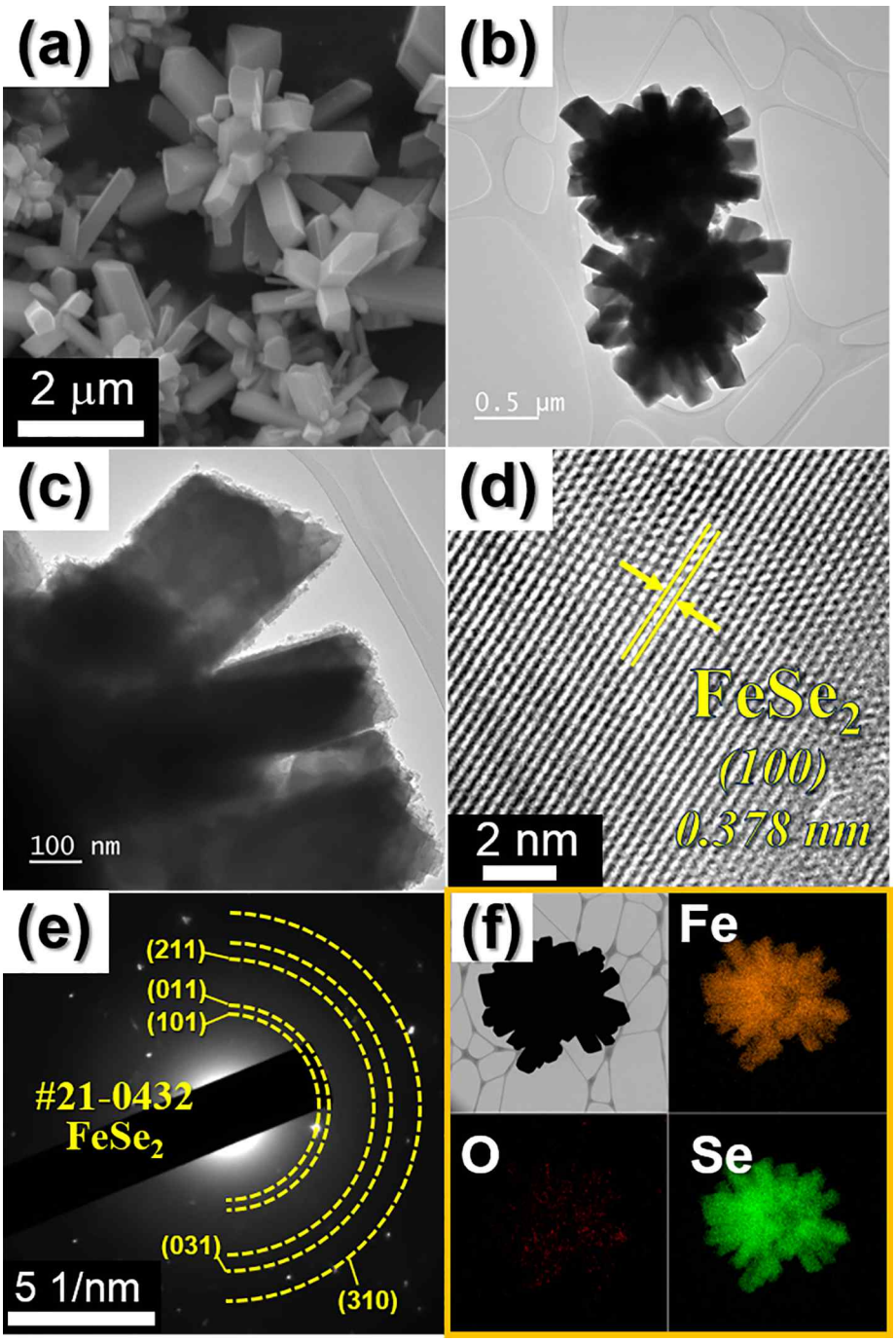


**Fig. S1** Morphologies and crystal structure of $FeSe_2$ rod clusters: (a) SEM image, (b, c) TEM images, (d) HR-TEM image (e) SAED pattern, and (f) elemental mapping images.

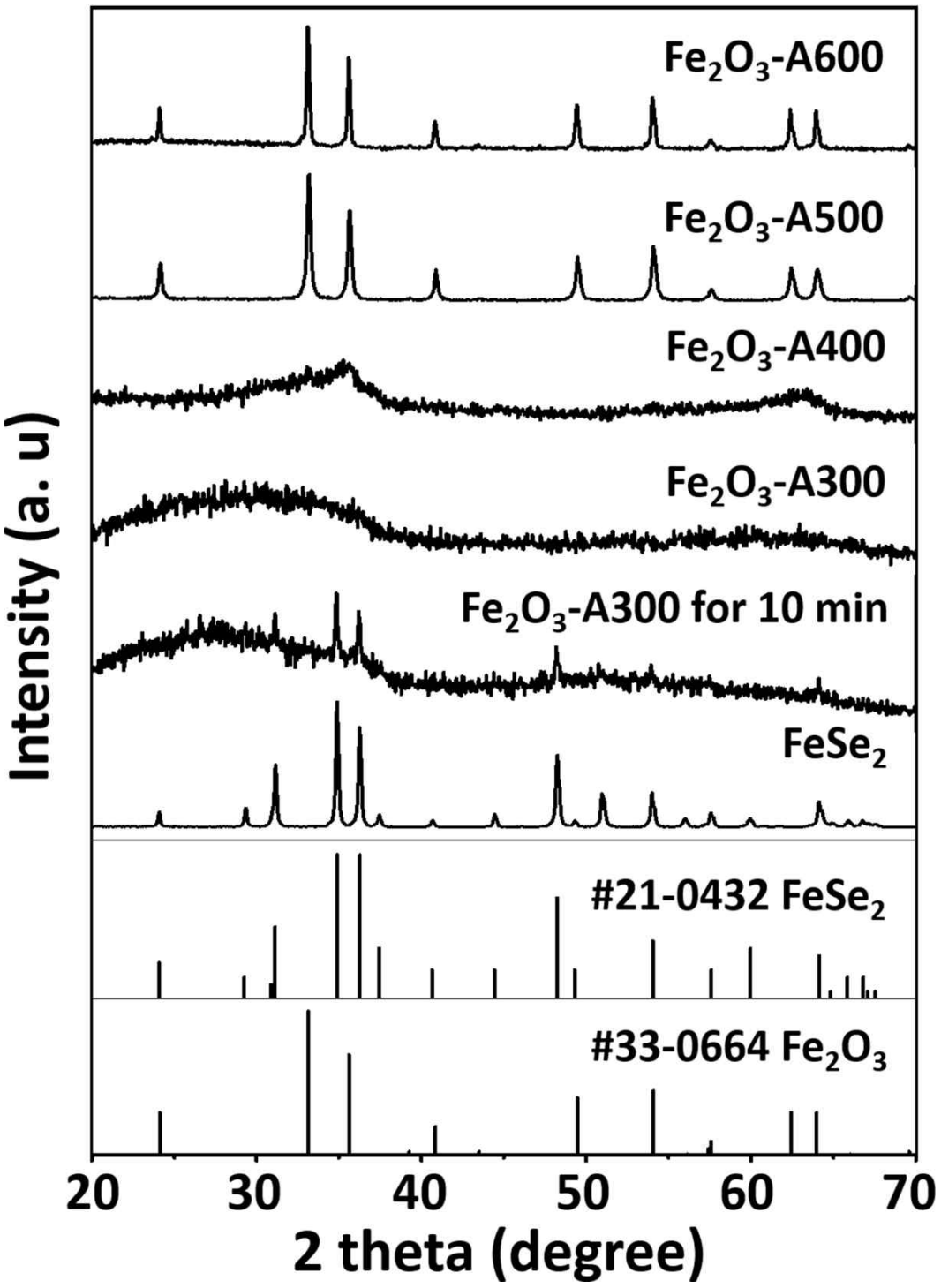


**Fig. S2** XRD patterns of $FeSe_2$, $Fe_2O_3$-A300 oxidized for 10 min, and $Fe_2O_3$-A300, -A400, -A500, and -A600 rod clusters oxidized for 3 hrs.

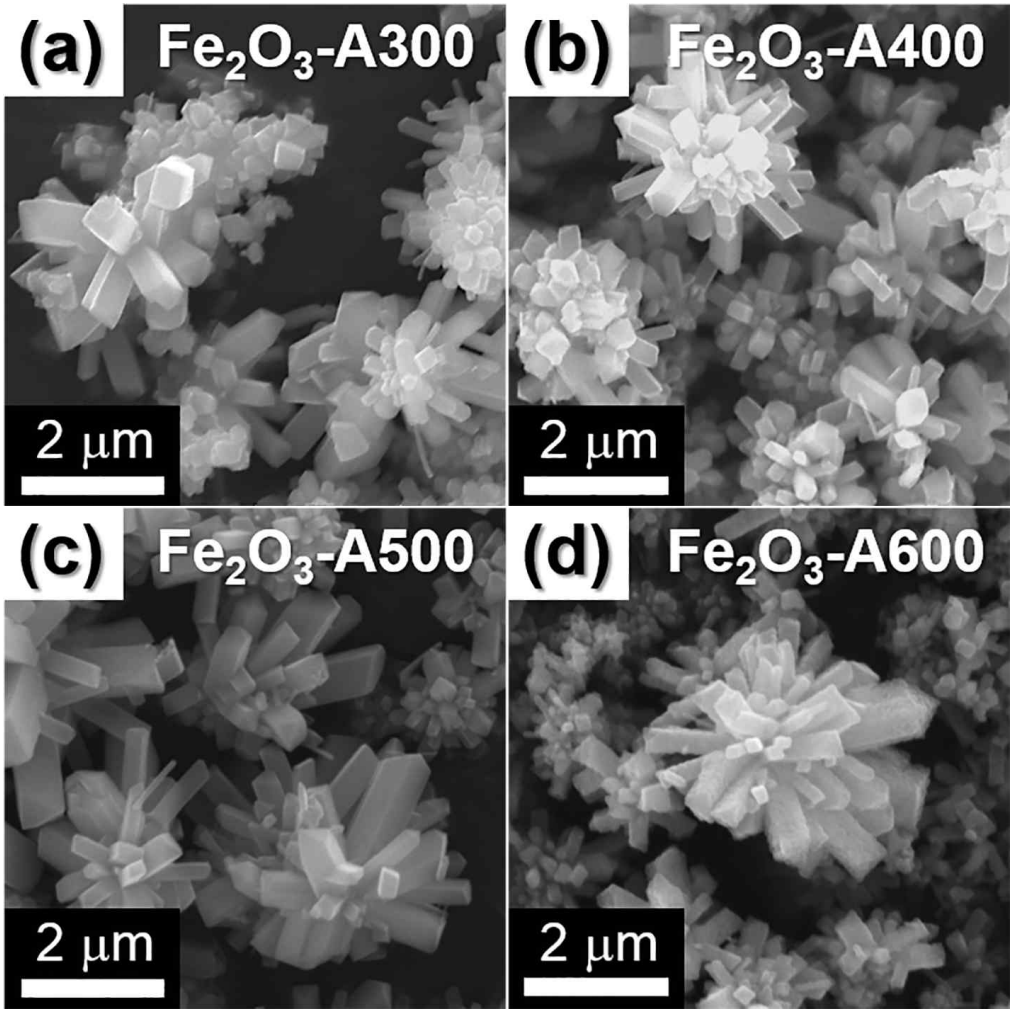


**Fig. S3** SEM images of $Fe_2O_3$-A300, -A400, -A500, and -A600 rod clusters.

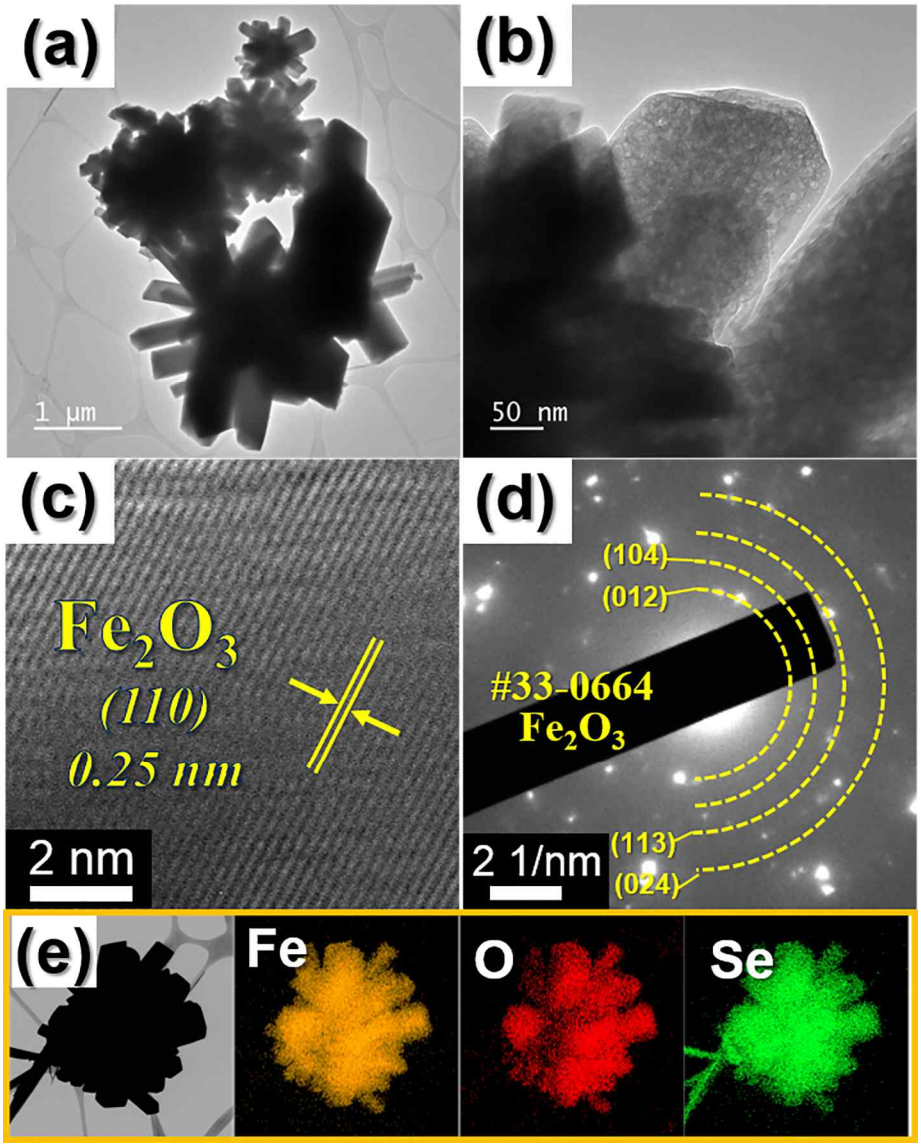


**Fig. S4** Morphologies and crystal structure of $Fe_2O_3$-A300 rod clusters: (a, b) TEM images, (c) HR-TEM image (d) SAED pattern, and (e) elemental mapping images.

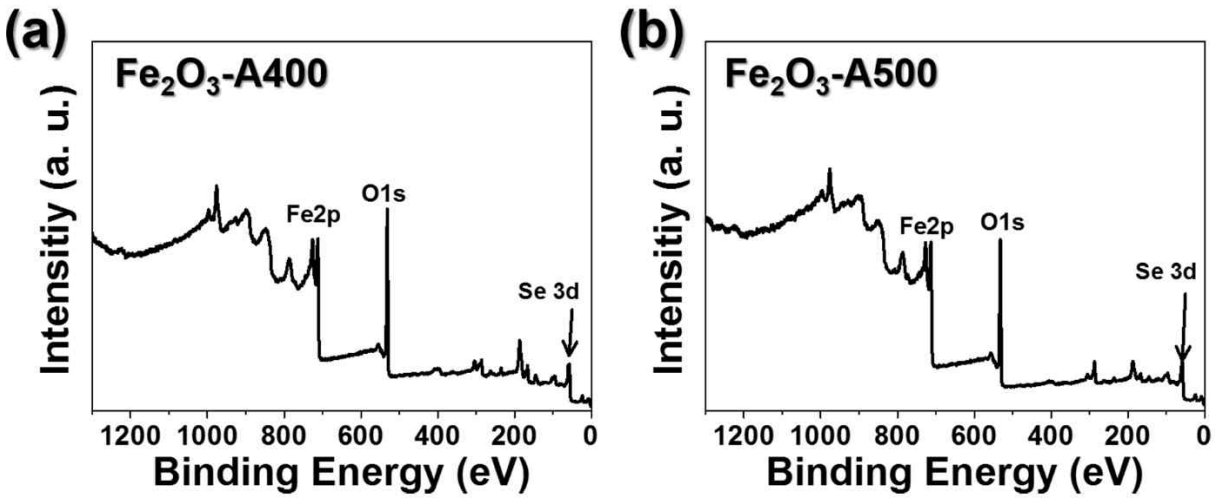


**Fig. S5** XPS survey scan of (a) $Fe_2O_3$-A400 and (b) $Fe_2O_3$-A500 rod clusters.

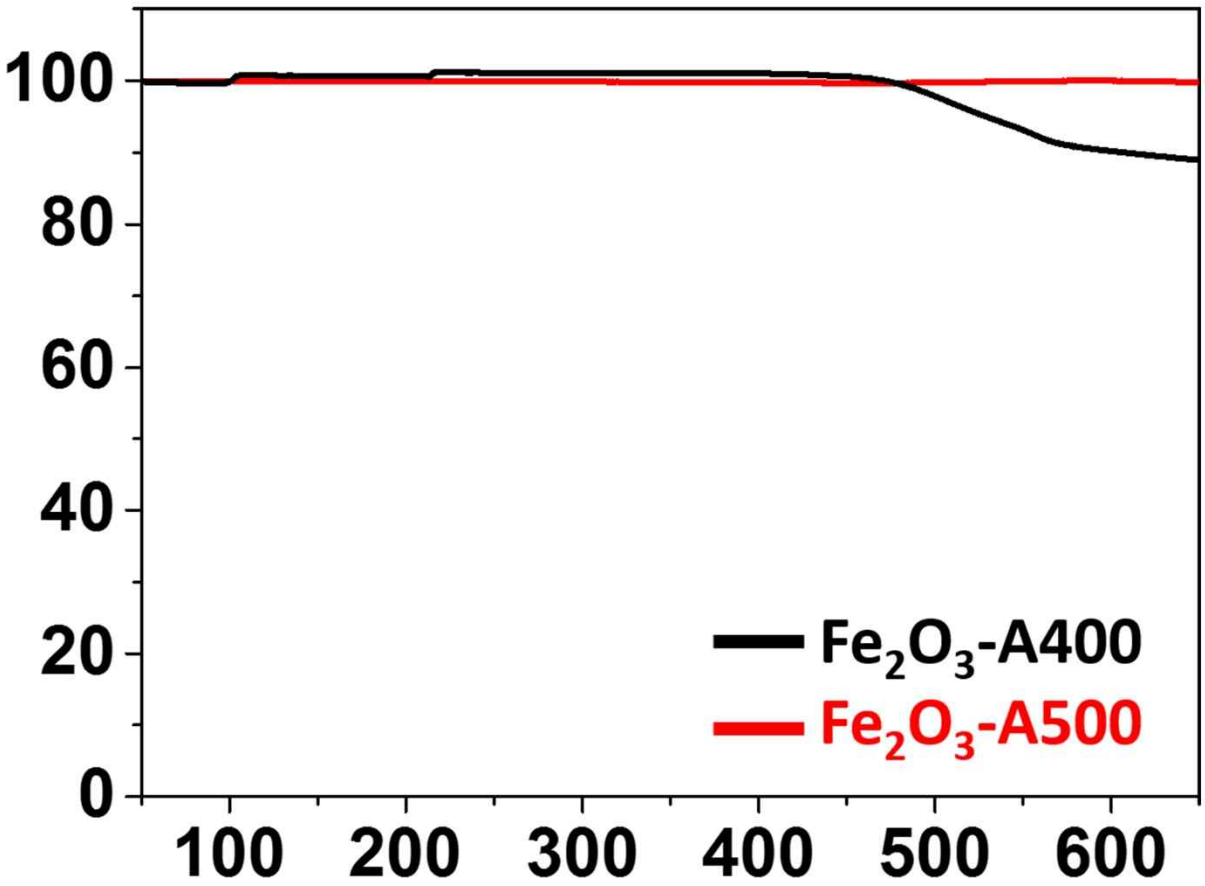


**Fig. S6** TGA curves of $Fe_2O_3$-A400 and -A500 rod clusters.

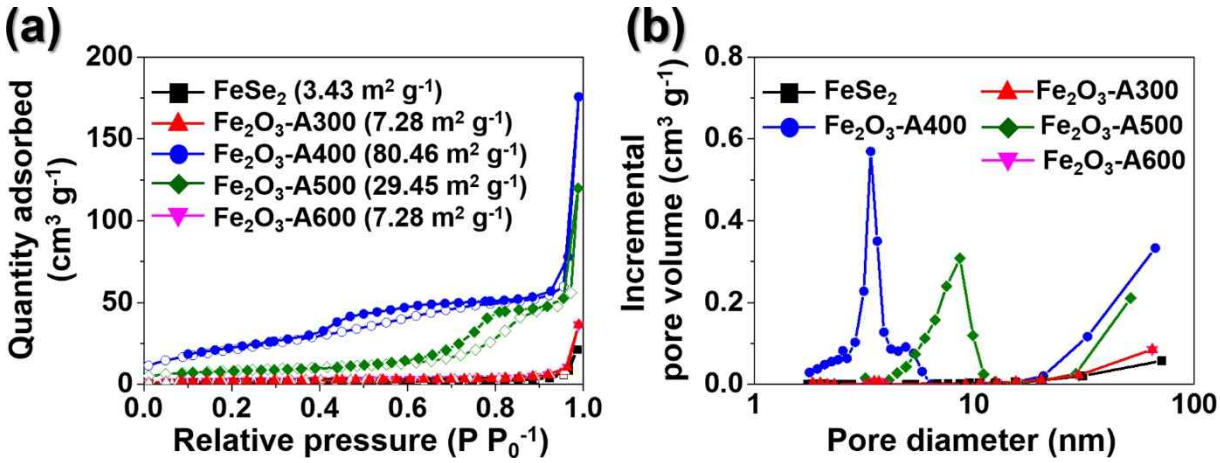


**Fig. S7** (a) $N_2$ adsorption and desorption isotherms and (b) BJH pore size distributions of $FeSe_2$, $Fe_2O_3$-A300, -A400, -A500, and -A600 rod clusters.

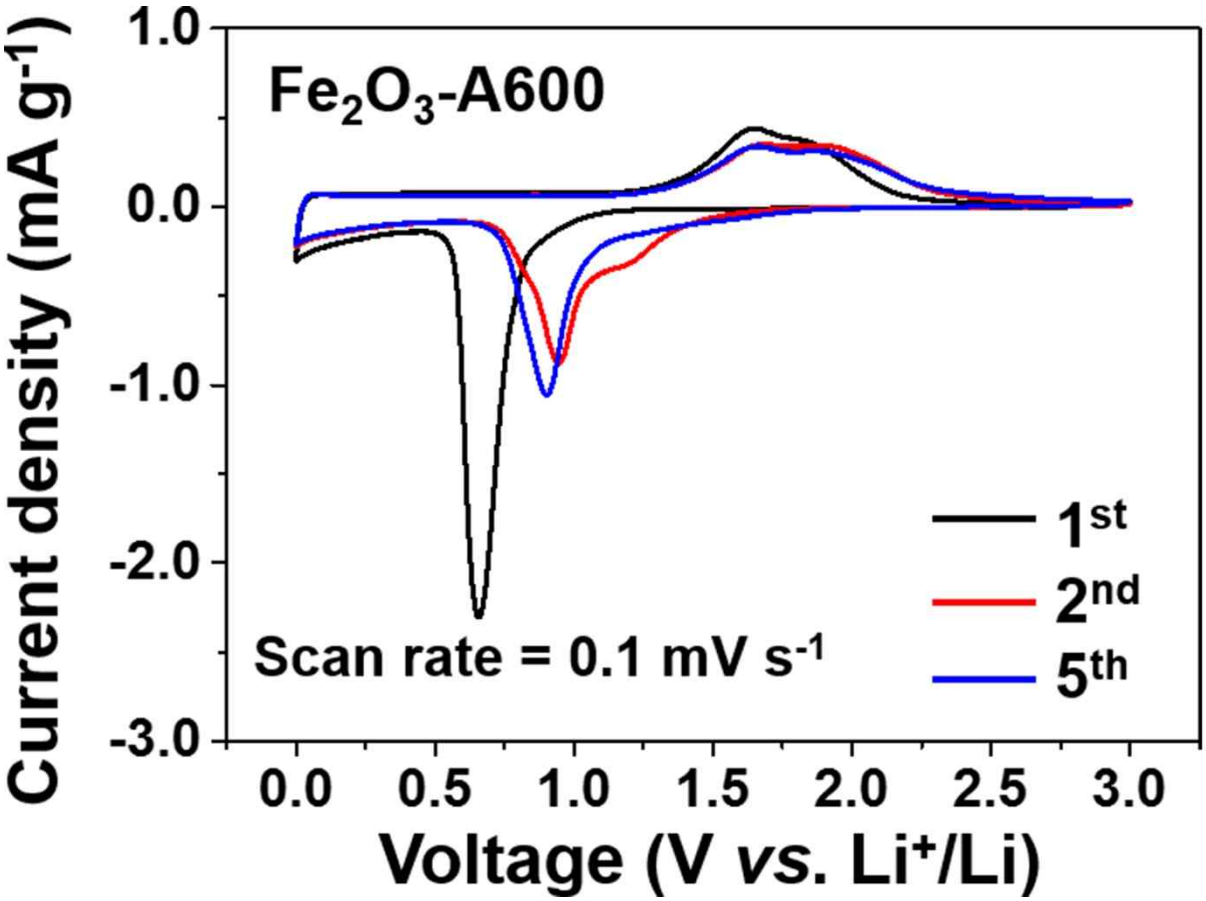


**Fig. S8** CV curves of $Fe_2O_3$-A600 rod clusters obtained at 0.1 mV $s^{-1}$ in the potential range of 0.001 – 3.0 V for the first, second, and fifth cycles.

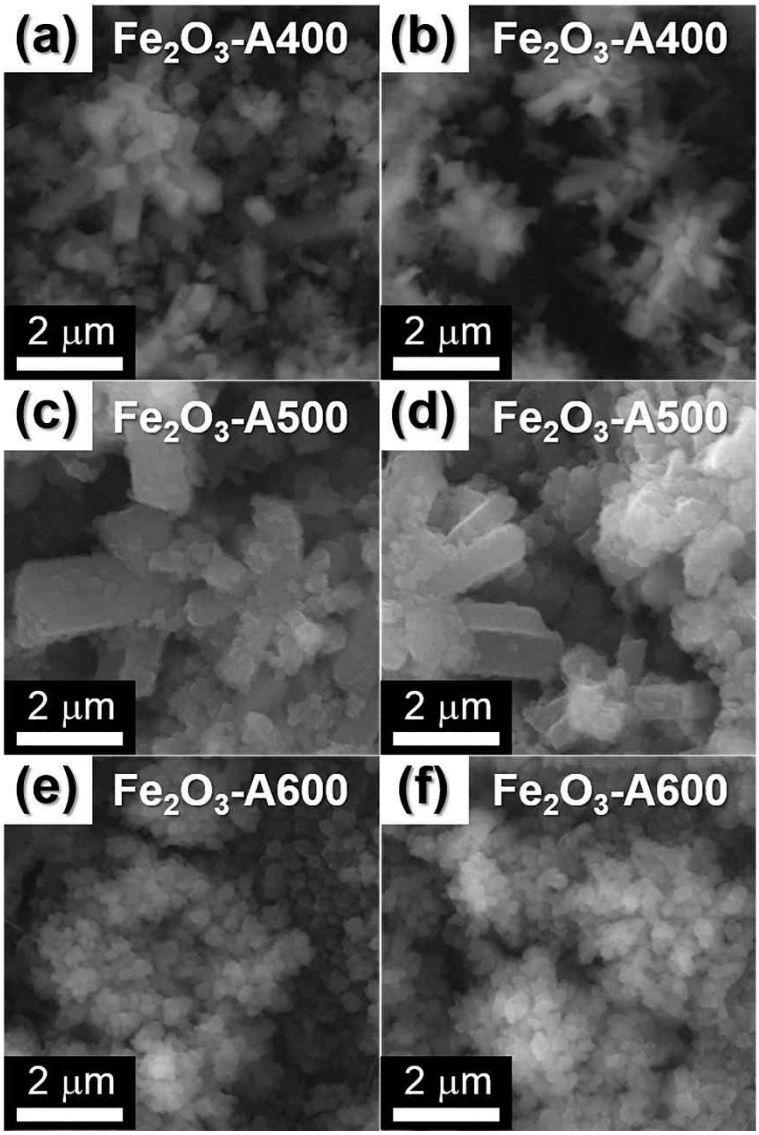


**Fig. S9** SEM images of (a, b) $Fe_2O_3$-A400, (c, d) -A500, and (e, f) -A600 rod clusters after 100 cycles.

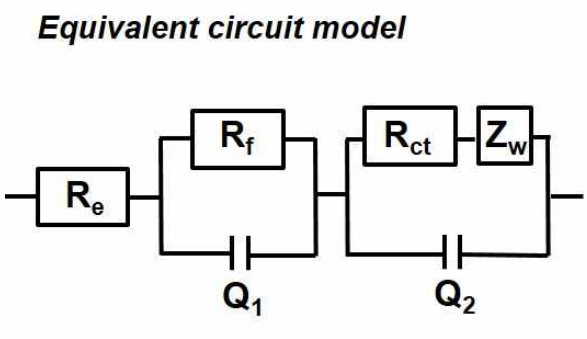


$R_e$: the electrolyte resistance, corresponding to the intercept of high frequency semicircle at Z' axis

$R_f$: the SEI layer resistance corresponding to the high-frequency semicircle

$Q_1$: the dielectric relaxation capacitance corresponding to the high-frequency semicircle

$R_{ct}$: the denote the charger transfer resistance related to the middle-frequency semicircle

$Q_2$: the associated double-layer capacitance related to the middle-frequency semicircle

$Z_w$: the Li-ion diffusion resistance

**Fig. S10** Randle-type equivalent circuit model used for AC impedance fitting.

**Table S1.** Chemical composition of $FeSe_2$, and $Fe_2O_3$-A300, -A400, -A500, and A600 rod clusters (based on the EDX quantitative data)

| Samples | Fe (wt %) | Se (wt %) | O (wt %) | Total |
|---|---|---|---|---|
| $FeSe_2$ rod clusters | 28.5 | 71.2 | 0.3 | 100 |
| $Fe_2O_3$-A300 | 44.1 | 38.4 | 17.5 | 100 |
| $Fe_2O_3$-A400 | 65.0 | 7.7 | 27.3 | 100 |
| $Fe_2O_3$-A500 | 69.4 | 1.4 | 29.2 | 100 |
| $Fe_2O_3$-A600 | 70.2 | 0.0 | 29.8 | 100 |

**Table S2.** Electrochemical properties of the $Fe_2O_3$ materials with various structures as anode materials for LIBs.

| Materials | Voltage range [V] | Current rate [A $g^{-1}$] | Discharge capacity after cycling [mA h $g^{-1}$] | Rate capability [mA h $g^{-1}$] /[A $g^{-1}$] | Ref |
|---|---|---|---|---|---|
| ***Porous $Fe_2O_3$ rod clusters*** | ***0.001 – 3.0*** | ***1.0*** | ***1381 ($200^{th}$)*** | ***745 (10.0 A $g^{-1}$)*** | ***Our work*** |
| Hollow $Fe_2O_3$ spheres | 0.05-3.0 | 0.2 | 710 ($100^{th}$) | - | 1 |
| Hierarchical hollow spheres composed of $Fe_2O_3$ nanosheets | 0.01-3.0 | 0.5 | 815 ($200^{th}$) | 330 (5.0 A $g^{-1}$) | 2 |
| Hierarchical $Fe_2O_3$ microboxes | 0.005-3.0 | 0.2 | 945 ($30^{th}$) | - | 3 |
| Hollow $Fe_2O_3$ nanospheres | 0.01-3.0 | 0.25 | 490 ($50^{th}$) | - | 4 |
| Hollow $Fe_2O_3$ nanobarrels | 0.01-3.0 | 0.5 | 916 ($100^{th}$) | 403 (10.0 A $g^{-1}$) | 5 |
| Multi-shelled hollow $Fe_2O_3$ spheres | 0.05-3.0 | 0.4 | 861 ($50^{th}$) | 294 (4.0 A $g^{-1}$) | 6 |
| Graphene-constructed hollow $Fe_2O_3$ spheres | 0.01-3.0 | 0.1 | 950 ($50^{th}$) | 640 (1.0 A $g^{-1}$) | 7 |
| Carbon coated hollow $Fe_2O_3$ sphere | 0.01-3.0 | 0.3 | 950 ($100^{th}$) | - | 8 |
| $Fe_2O_3$ nanorods | 0.005-3.0 | 0.5 | 970 ($100^{th}$) | 300 (5.0 A $g^{-1}$) | 9 |
| Spindle-like $Fe_2O_3$ | 0.01-3.0 | 0.2 | 911 ($50^{th}$) | 424 (10.0 A $g^{-1}$) | 10 |
| $Fe_2O_3$ nanoparticle-loaded carbon nanofibers | 0.05-2.8 | 0.05 | 488 ($75^{th}$) | 288 (0.5 A $g^{-1}$) | 11 |
| $Fe_2O_3$ nano-assembled spindles | 0.005-3.0 | 0.1 | ~900 ($40^{th}$) | 430 (1.0 A $g^{-1}$) | 12 |

## References


1. B. Wang, J. S. Chen, H. B. Wu, Z. Y. Wang and X. W. Lou, *J. Am. Chem. Soc.*, 2011, **133**, 17146-17148.
2. J. X. Zhu, Z. Y. Yin, D. Yang, T. Sun, H. Yu, H. E. Hoster, H. H. Hng, H. Zhang and Q. Y. Yan, *Energy Environ. Sci.*, 2013, **6**, 987-993.
3. L. Zhang, H. B. Wu, S. Madhavi, H. H. Hng and X. W. Lou, *J. Am. Chem. Soc.*, 2012, **134**, 17388-17391.
4. M. Sasidharan, N. Gunawardhana, M. Yoshio and K. Nakashima, *Ionics*, 2013, **19**, 25-31.
5. K. S. Lee, S. Park, W. Lee and Y. S. Yoon, *ACS Appl. Mater. Interfaces*, 2016, **8**, 2027-2034.

6. Z. Padashbarmchi, A. H. Hamidian, H. W. Zhang, L. Zhou, N. Khorasani, M. Kazemzad and C. Z. Yu, *RSC Adv.*, 2015, **5**, 10304-10309.
7. Y. W. Chen, J. Z. Wang, J. Z. Jiang, M. A. Zhou, J. Zhu and S. Han, *RSC Adv.*, 2015, **5**, 21740-21744.
8. Z. J. Du, S. C. Zhang, J. F. Zhao, X. M. Wu and R. X. Lin, *J. Nanosci. Nanotechno.*, 2013, **13**, 3602-3605.
9. Y. M. Lin, P. R. Abel, A. Heller and C. B. Mullins, *J. Phys. Chem. Lett.*, 2011, **2**, 2885-2891.
10. X. Xu, R. Cao, S. Jeong and J. Cho, *Nano Lett.*, 2012, **12**, 4988-4991.
11. L. W. Ji, O. Toprakci, M. Alcoutlabi, Y. F. Yao, Y. Li, S. Zhang, B. K. Guo, Z. Lin and X. W. Zhang, *ACS Appl. Mater. Interfaces*, 2012, **4**, 2672-2679.
12. A. Banerjee, V. Aravindan, S. Bhatnagar, D. Mhamane, S. Madhavi and S. Ogale, *Nano Energy*, 2013, **2**, 890-896.